Optimal Size Regime for Oxidation-Resistant Silicon Quantum Dots

Huashan Li, Mark T. Lusk,* Reuben T. Collins, and Zhigang Wu*

Department of Physics, Colorado School of Mines, Golden, Colorado 80401, United States

ABSTRACT First-principles computations have been carried out to predict that appropriately terminated silicon quantum dots with diameters in the range of 1.2−2 nm will offer a superb resistance to oxidation. This is because surface treatments can produce dangling bond defect densities sufficiently low that dots of this size are unlikely to have any defect at all. On the other hand, these dots are large enough that the severe angles between facets do not expose bonds that are vulnerable to subsequent oxygen attack. The absence of both surface defects and geometry-related vulnerabilities allows even very short passivating ligands to generate an effective barrier, an important consideration for charge and exciton transport within quantum dot assemblies. Our computations, which employ many-body perturbation theory using Green functions, also indicate that dots within this size regime have optical and electronic properties that are robust to small amounts of inadvertent oxidation, and that any such oxygen incorporation is essentially frozen in place.

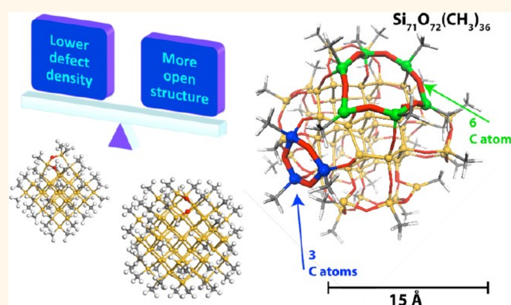

KEYWORDS: oxidation · Si quantum dot · passivation · transition state · optical absorption · photovoltaics

Because of their tunable optical gaps and high absorption cross sections, quantum-confined silicon quantum dots (Si QDs) have been extensively studied over the past decade as a promising material for photovoltaic and photoluminescence applications. In addition, their size can influence both the nanostructural morphology and energy level alignments to improve the corresponding metrics of short circuit current and open circuit voltage.[1] Further efficiencies might even be realized because Si QDs are known to facilitate multiple exciton generation (MEG).[2]

Despite offering a panoply of promising properties, the oxidation of quantum dots is a primary obstacle to their incorporation in new technologies. While bulk silicon will self-passivate with a stable oxide layer of approximately 3 nm,[3] such a layer would amount to the complete oxidation of quantum-confined Si QDs.

For the largest of quantum-confined dots, the oxide shell generates an interfacial stress which mechanically restricts further oxidation. For example, a stable 1.2 nm oxidation shell measured for a 5 nm dot has been attributed to such stress-induced stasis.[3−5] For smaller QDs, however, the entire structure would be oxidized because the requisite interfacial stress cannot be generated.[3] In any case, even a thin oxide layer can have significant optical and electronic consequences, in particular, on altering photoluminescence.[4]

The oxidation of Si QDs is perceived as being increasingly problematic as their size decreases because of its greater impact on optical and electronic properties.[6−11] This is unfortunate because there are several motivations to push for monodispersed assemblies at the small end of the quantum-confined range. For instance, MEG efficiency increases as dot size decreases[12] and so does the efficiency of exciton transport.[13] In addition, smaller dots imply a more significant role for surface termination, opening up the design space even further. It is therefore critical to identify a means of preventing the oxidation of quantum-confined Si QD, in particular, for dots in the range of 1−2 nm.

A reasonable starting point is to consider passivation strategies that work well on planar Si surfaces. Provided that they have sufficient kinetic energy to overcome any energetic barriers encountered, O_2 near such surfaces will dissociate, break a pair of nearby Si−Si bonds, and create new

* Address correspondence to mlusk@mines.edu, zhiwu@mines.edu.

Received for review July 11, 2012 and accepted October 14, 2012.

Published online October 15, 2012
10.1021/nn303109t

© 2012 American Chemical Society

Si−O−Si arrangements. Terminating groups are chosen to increase the energy barriers associated with this process. For instance, hydrogen is a common Si passivant even though O_2 can dissociate and form Si−O−Si at back bonds in a single step that has a negligible barrier at room temperature.[14] This barrier increases rapidly with surface coverage, though, and because the mobility of O is low, it is possible to achieve stable surfaces that exhibit submonolayer O coverage.[14] Significantly, this level of protection is only achieved in the *absence of surface defects*.[15] Surface dangling bonds, in particular, can greatly reduce the dissociative barrier (E_a^{dis}) for O adsorption. An alternative to hydrogen is methyl termination which has an initial $E_a^{dis} > 2.5$ eV,[14] but this value presumes an absence of surface defects as well. The same defect issue arises for termination groups, such as siloxanes, which are expected to otherwise provide superb shield for Si QDs.[16−19]

The defect issue can be covered up by using longer ligands, through which oxygen must penetrate to reach the defect, for achieving a more robust layer of protection. However, the photovoltaic (PV) applications with QDs cannot afford this luxury; the ligand must be short enough to ensure sufficient charge mobility in Si QD networks to efficiently collect photoexcited carriers.[20,21] An alternate strategy must therefore be invoked wherein the defects themselves are eliminated to the greatest possible extent, allowing short ligands to adequately protect the QD surfaces.

Recent electron paramagnetic resonance (EPR) experiments with H-terminated Si QDs on the large side of the 1−5 nm range indicate that their dangling bond densities are typically very high. Quenching of the EPR signal, as well as the reappearance of light emission on short time scales after exposure to ambient environment, reflects a corresponding rapid initial oxidation at these surface defect sites for H passivation.[22−26] For both dots and bulk surfaces, the density of these defects can be reduced by orders of magnitude with proper surface treatment, but this defect density in dots translates into a logarithmic relationship between dot diameter and the number of defects. EPR analysis has been used to quantify the relation between the number of surface dangling bonds, N_{DB}, and dot diameter, d.[27] For dots subjected to a combination of either hydrogen fluoride (HF) etching and annealing or HF etching and hydrosilylation, the reported relation is

$$N_{DB} = 2.0 \times 10^{-4} d^3 \qquad (1)$$

with the dot diameter given in nanometers. This fit is shown in Figure 1 along with the original data points from Niesar *et al.*[27] In assemblies of 2 nm dots, then, only one in a thousand will have dangling bond defects. It is worth emphasizing that the surface defect density resulting from the HF plus hydrosilylation treatment is not size-dependent, implying that QD

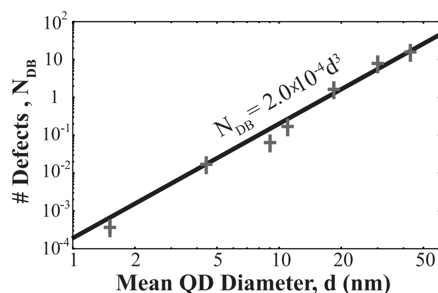

Figure 1. Number of dangling bond defects per Si QD as a function of the mean dot diameter for HF + annealed treated Si QDs.[27]

assemblies can be generated for which most of the dots have no defects at all.

The solution to QD oxidation would apparently be to make dots sufficiently small so that their defect-free surfaces can be adequately passivated with short ligands. However, the surfaces of small dots have facets meeting at more severe angles; therefore, they expose vulnerable bonds that are rapidly oxidized even in the absence of any defects. For instance, the oxidation rate of dots with diameters of less than 5 nm was observed to be significantly greater than that for bulk Si.[4,7,28] We therefore seek to identify the size range of quantum-confined Si QDs for which there are neither surface defects nor geometry-induced oxidation vulnerabilities. A first-principles computational approach is used to consider 1−2 nm Si QDs terminated by hydrogen (H), CH_3, and siloxane networks. Within this setting, the oxidation barriers for three activated processes are calculated: adsorption of oxygen molecules; lateral hopping of adsorbed O; and inward hopping of adsorbed O.

Our results indicate that any O adsorbed onto the surfaces of extremely small dots ($d <$ nm) will be frozen within Si backbonds. However, there exist many susceptible entry points for O incorporation into the dot structure, and this is independent of the terminating surface group considered. The adsorption barrier for these vulnerable sites increases sharply with dot size, though, exhibiting a very fast convergence toward that of the bulk surface. Pragmatically speaking, properly treated dots with diameters greater than 1.2 nm, which are subsequently terminated with CH_3 or siloxanes, will be unlikely to oxidize at room temperature on meaningful application time scales. Since less than one out of a thousand such dots with $d < 2$ nm would have surface defects,[27] we conclude that the 1.2−2 nm size range is optimal for optoelectronic applications. Furthermore, our computations show that a small amount of inadvertent oxidation of methyl-terminated dots will have a negligible effect on their optical gaps and will actually enhance the band edge optical absorption.

RESULTS AND DISCUSSION

In contrast to bulk Si, the surface atoms of Si QDs have distinct local geometries that react differently to

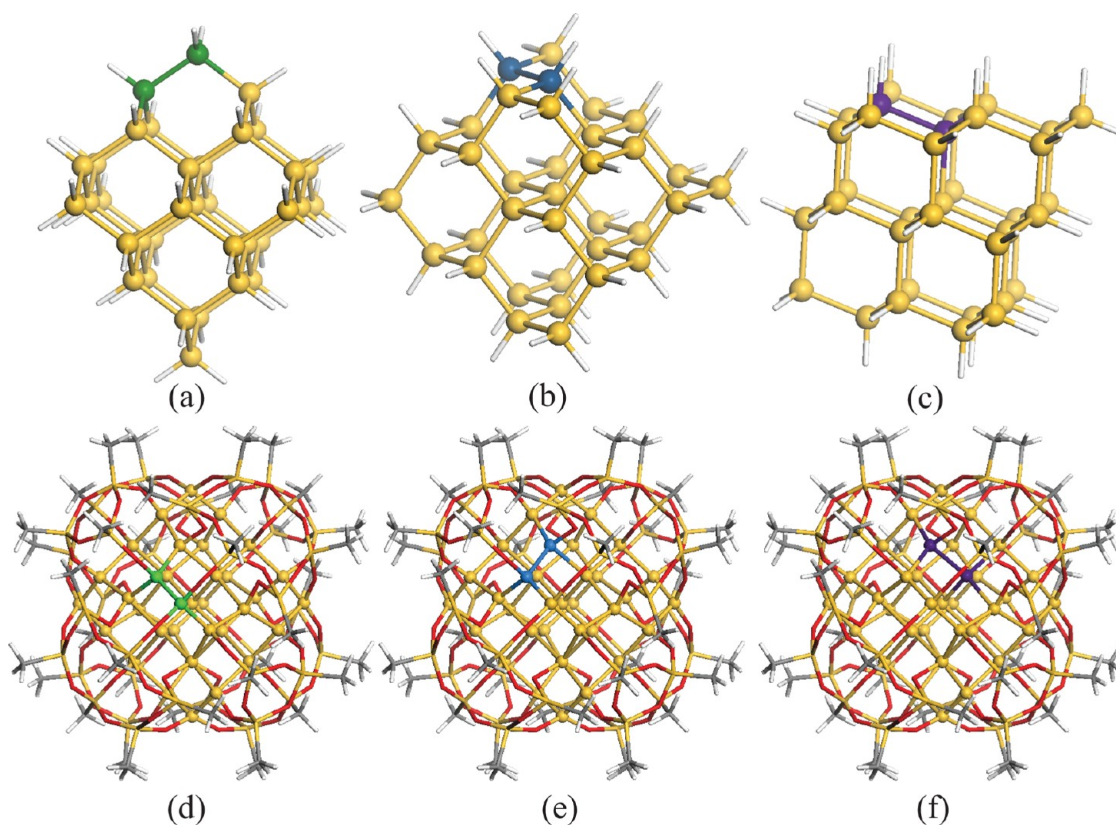

Figure 2. Three types of inequivalent surface bonds on H (a–c) and siloxane network (d–f) terminated Si_{35}: apex (green), ridge (blue), and face (purple). The remaining Si atoms are tan, H atoms are white, C atoms are gray, and O atoms are red.

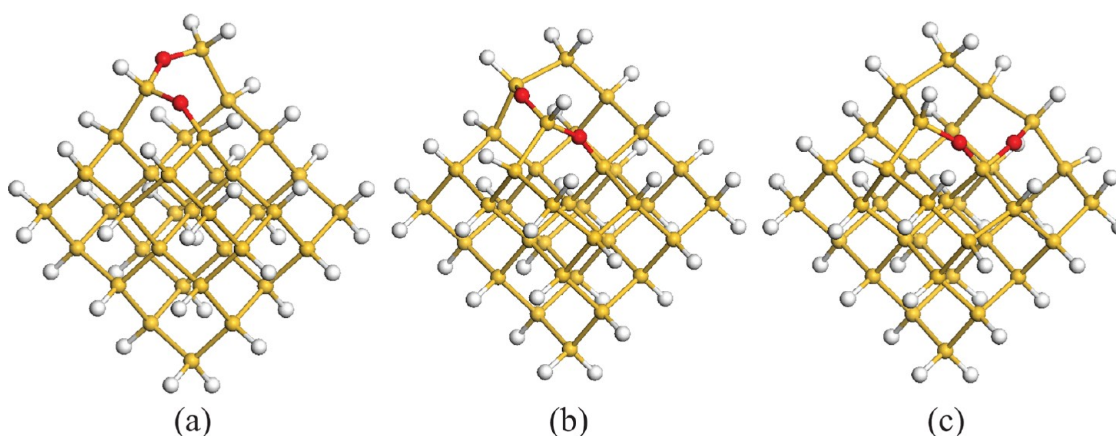

Figure 3. Final state configurations of three barrierless dissociative adsorption paths for the first O_2 on $Si_{35}H_{36}$.

the presence of oxygen. In particular, these atoms can be shared by one, two, or three surface facets. Our calculations indicate that corner sites (those shared by three facets) are the most vulnerable to oxidation while those shared only by one facet are the most resistant. As the dot size increases, the percentage of corner sites reduces dramatically, resulting in sharply enhanced resistance to oxidation. We show this first for Si_{35} dots (d = 1.0 nm) that turn out to be too small to resist oxygen attack. Dots only slightly bigger though, the Si_{66} dots (d = 1.2 nm), are then analyzed and found to offer oxidation resistance very similar to that of defect-free, bulk surfaces. Three passivants are considered: hydrogen, methyl, and siloxane networks. We have also investigated the lateral and inward diffusion of O atoms adsorbed onto these two dots and compared the associated optical and electronic properties with those that are free of any oxygen.

Si_{35} Dots Are Vulnerable. The Si_{35} dots have only three types of inequivalent surface bonds, *apex*, *ridge*, and *face*, as illustrated in Figure 2. Each of these can be oxidized through barrierless direct dissociative paths

that result in pairs of Si−O−Si bonds, and the configurations of the three final states with O atoms sitting at the Si−Si backbonds are shown in Figure 3. The coverage dependence of activation energy was also investigated by considering geometries wherein all but one pair of surface bonds are oxidized. The activation barriers are still zero so that O coverage offers no additional protection to these vulnerable sites.

The situation is different for CH_3-passivated dots of the same size, $Si_{35}(CH_3)_{36}$, because the much stronger steric repulsion between CH_3 ligands and the incoming O_2 molecule forces the oxidation of back bonds to become a three-step process, as shown in Figure 4: (i) formation of C−O−O−H intermediate by inserting O_2 to the C−H bond; (ii) decomposition of C−O−O−H into C−OH and C═O intermediates; and (iii) hopping of O atoms from the ligand to Si−Si backbonds. Here it is

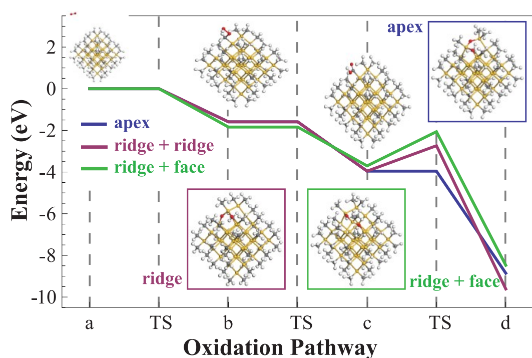

Figure 4. Energy diagram of three-step reaction paths for O_2 incorporation in $Si_{35}(CH_3)_{36}$ with transition states labeled as TS: (a) O_2 far away from the dot; (b) formation of C−O−O−H intermediate; (c) formation of C−OH or C═O intermediates; and (d) insertion of O into the Si core. The inset figures with blue, red, and green frames present the final state configuration of the associated paths with the same color. The small inset figures show the initial and intermediate structures.

only the apex sites that are vulnerable, offering no barrier to oxidation. The total barriers (E_a^{dis}) for ridge/ridge and ridge/face oxidation are 1.2 and 1.6 eV, respectively. Aside from the geometry-induced apex site vulnerability, methyl passivation therefore provides much better protection against oxidation than does H, in agreement with our previous analysis of bulk Si surfaces.[14] The coverage dependence of apex oxidation was investigated by allowing oxygen to occupy back bond sites on five of the six apexes, as illustrated in Figure 5. Oxidation attack on the remaining apex site was found to have a barrierless second step, but the activation energies for the first and third steps rise to 1.3 and 0.7 eV, respectively. This is due to the more compact structure of both ligands and back bonds around the initially unoxidized apex bond.

In general, processes that must overcome a barrier greater than 1.2 eV are unlikely to occur in an ambient environment, using a characteristic reaction time (Table 1) at room temperature estimated by the Arrhenius equation with the prefactor of $10^{13}-10^{15}$ s^{-1}.[15]

For both H and CH_3 passivation, each hydrogen or methyl is bonded to individual Si atoms, a termination referred to as being "zero-dimensional". Siloxane networks,[16−19] on the other hand, can be of higher dimension such as the "one-dimensional" scheme shown in Figure 6 (left and right panels). Here, terminating moieties bridge between pairs of Si atoms, in this case characterized by triangular and hexagonal ring networks. This complex passivation scheme exhibits three types of surface bonds for Si_{35}, as shown in Figure 2d−f. Similar to the methyl passivation, the apex bonds can be attacked by O_2 through a barrierless dissociative path, but the remaining 75% of surface bonds are well-shielded by the siloxane cap. Like the methyl-passivated dots, ridge bonds offer a higher

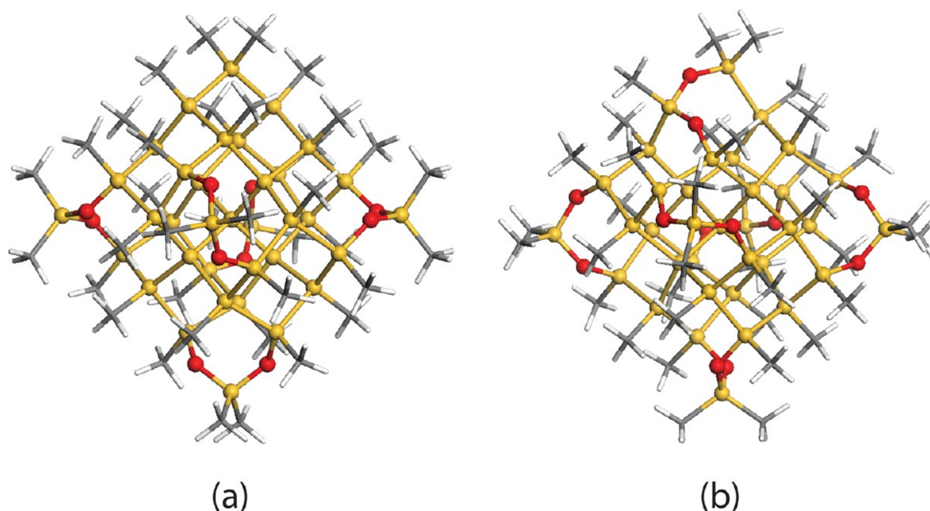

Figure 5. Initial and final configurations of O_2 incorporation into $Si_{35}(CH_3)_{36}O_{10}$ with all but one pair of the apex bonds oxidized in the initial configuration and the last apex site oxidized in the final configuration.

resistance to oxidation than do apex bonds. For dots with high geometry-induced vulnerability, the protection offered by such siloxane networks will correlate with the degree to which the network is able to form an encompassing shield.

Si_{66} Dots Are Protected. The QD surface exposes vulnerable bonds, so the barriers to oxidation are not expected to ever exceed those of planar surfaces. This is certainly the case for hydrogen passivation, where planar surfaces do not offer a barrier to initial oxygen attack,[14] and $Si_{66}H_{64}$ dots were found to be vulnerable at all sites. However, the vulnerability induced by QD surface geometry that is observed for methyl-passivated apex bonds is not present in those only slightly larger in size. In contrast to the smaller dots, and in keeping with bulk surface treatments, only partial coverage with methyl is possible due to steric hindrance. For instance, $Si_{66}(CH_3)_{40}H_{24}$ dots offer an apex site barrier of 2.3 eV, close to the bulk value of 3.0 eV for methyl-terminated flat Si(111) surfaces.[14] Figure 7 compares the energy profiles for methyl-passivated Si_{35}, Si_{66}, and a Si(111) surface. Larger facet angles at QD surfaces rapidly increase the barriers to the first two oxidation steps due to steric repulsion, except that $Si_{66}(CH_3)_{40}H_{24}$ offers the highest barrier in the third oxidation step as a result of the surface geometry-induced compression of the Si−Si back bonds.

TABLE 1. Activation Energy and Its Characteristic Time at 293 K Calculated Using the Arrhenius Equation[a]

E_a (eV)	τ_1	τ_2
1.2	506 days	5 days
1.1	10 days	2 h
1.0	4 h	3 min
0.9	5 min	3 s

[a] Characteristic times τ_1 and τ_2 are associated with prefactors of 10^{13} and 10^{15} s^{-1}, respectively.

This has remarkable implications for the protection of QDs from oxidation. Just as for bulk surfaces, hydrogen passivation does not offer any barrier to initial oxidation,[14] although the barrier increases rapidly with the surface coverage of oxygen in both settings. For methyl and siloxane passivation, only Si QDs with a diameter less than 1.2 nm will be oxidized significantly faster than bulk Si surfaces, while QDs with $d > 1.2$ nm provide strong oxidation resistance nearly identical to that of (defect-free) bulk surfaces. As reproduced in Figure 1 using Niesar's experimental data,[27] it is possible to prepare quantum dots in the 1.2−2 nm range so that only one dot in a thousand has surface defects. Although these are for the H passivation, the resulting dots can be subsequently passivated with either methyl or siloxane networks. We therefore predict this to be a sweet spot size regime for the synthesis of robust Si QDs. This optimal size range of 1.2−2.0 nm is within the reach of current synthesis technologies. For example, Ozin's group has successfully separated the colloidally stable allylbenzene-capped silicon nanocrystals into several visible emitting monodisperse fractions in the range of 1−5 nm in diameter.[29]

Lateral and Inward Diffusion of O in Si QDs. Thus far, only the energy barriers to initial oxidation have been considered, but the experimentally measured *effective* energy barriers typically include lateral and inward diffusion of O atoms. Coverage-dependent barriers to

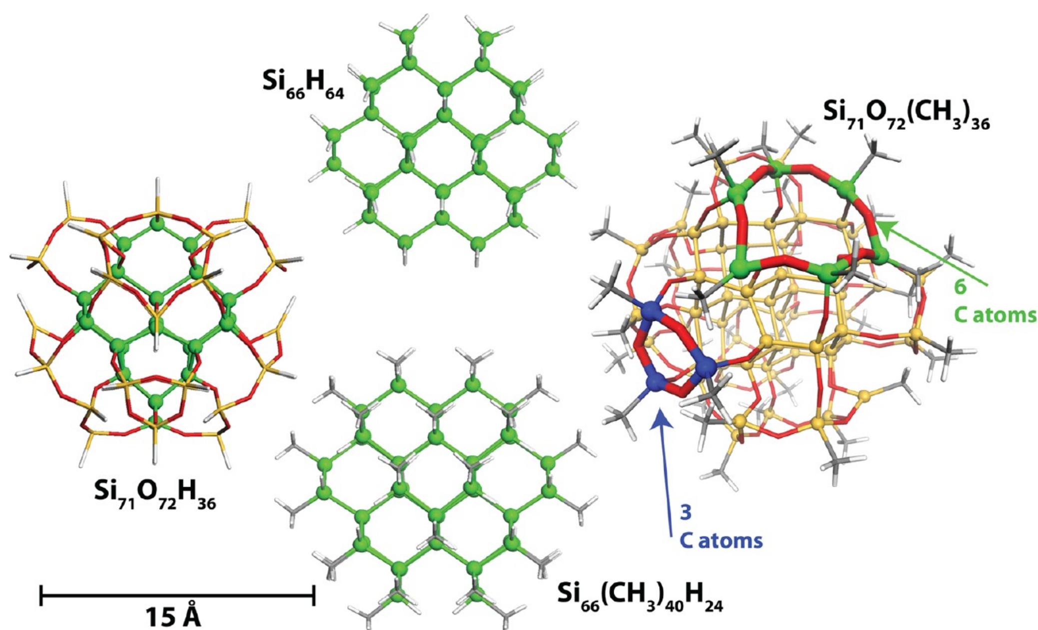

Figure 6. Small quantum-confined Si QDs illustrating passivation with H (top), CH_3 + H (bottom), and siloxane networks (left and right). Si atoms are shown in tan, green, and blue, O atoms are red, C atoms are gray, and H atoms are white.

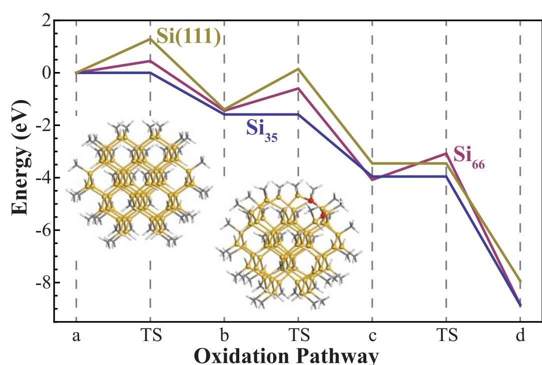

Figure 7. Energy diagram of three-step reaction paths for O_2 adsorption on $Si_{35}(CH_3)_{36}$, $Si_{66}(CH_3)_{40}H_{24}$, and CH_3-terminated Si(111) surface with transition states labeled as TS. The configuration of the system evolves with (a) O_2 far away from the dot; (b) formation of C−O−O−H intermediate; (c) formation of C−OH or C=O intermediates; and (d) insertion of O into the Si core. The insets are initial and final configurations for O_2 adsorption on an apex bond of $Si_{66}(CH_3)_{40}H_{24}$.

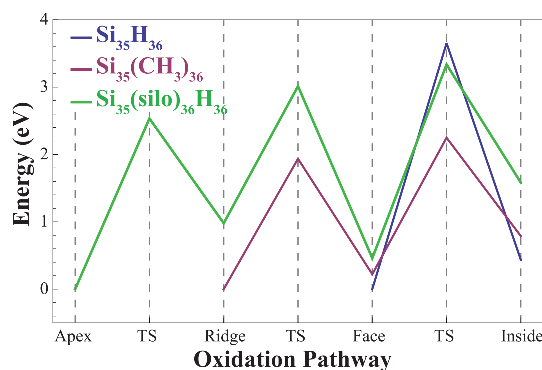

Figure 8. Energy diagram for accessing the hard-to-oxidize surface bonds and interior bonds on H, CH_3, and siloxane-terminated Si_{35} through progressive diffusion from susceptible sites: apex bonds (green), ridge bonds (blue), face bonds (purple), and interior bonds. TS indicates a transition state.

TABLE 2. Percent of Surface Oxidized, *P*, and Associated Effective Barrier, E_a (in eV), for Apex, Ridge, and Face Bonds of H, CH_3, and Siloxane-Terminated Si QDs (The Brackets Denote a Range of Barriers Where Multiple Pathways Exist)

Si QD	E_a^{apex}	P_{apex}	E_a^{ridge}	P_{ridge}	E_a^{face}	P_{face}
$Si_{35}H_{36}$	0.0	25.0	0.0	50.0	0.0	25.0
$Si_{35}(CH_3)_{36}$	0.0	25.0	(0.0,1.6)	50.0	1.6	25.0
$Si_{35}(silo)_{36}$	0.0	25.0	2.5	50.0	4.5	25.0

such motion can sharply decrease the rate at which first stage oxidation occurs, so the stability of small dots that have been partially oxidized is important to consider. Though computationally prohibitive, it would be useful to calculate a *global effective barrier* defined as the average of the energy barriers associated with a complete monolayer of QD oxidation. This could be directly compared with experimental data. Instead, we introduce a *local effective barrier* (E_a^{eff}) as the minimum activation energy for oxidizing a pair of neighboring Si bonds. This pragmatic reduction in scope can still be used to estimate trends associated with the global effective barrier. The requisite analysis is carried out for Si_{35}.

Geometric restrictions that derive from the proportion and arrangement of surface site types are of central importance in determining E_a^{eff} at each position on the surface. For example, there is no barrier for the oxidation of a single ridge site on $Si_{35}(CH_3)_{36}$, but there are 24 ridge bonds and only 12 apex bonds in total. As a result, complete oxidation of ridge sites requires other oxidation routes and/or surface hopping, and the resulting effective barrier is then greater than zero even with coverage dependence ignored.

Our analysis of $Si_{35}H_{36}$ indicates that E_a^{eff} is zero for all surface bonds on $Si_{35}H_{36}$, so all of these bonds will rapidly oxidize. As summarized in Table 2, if H is replaced with CH_3 or siloxane, the proportion of such barrierless sites reduces to 75 and 25%, respectively. The calculated values of E_a^{eff} could qualitatively explain the inhomogeneous surface oxidation observed in the evolution of the FTIR spectrum.[7] In addition, they also show a trend consistent with experimental results that siloxane offers the best protection to monolayer oxidation, followed by methyl and then hydrogen.[16,18,19,30]

Figure 8 summarizes the energy diagram for accessing the hard-to-oxidize surface bonds on H, CH_3, and siloxane-terminated Si_{35} through progressive diffusion from susceptible sites with zero barrier. Every hopping event is energetically unfavorable except for ridge-to-face hops on siloxane-terminated dots. The barriers to all lateral and inward hops are greater than 2 eV, implying that the O atoms are effectively frozen at room temperature.

Apex-to-ridge and ridge-to-face hops on $Si_{35}H_{36}$ have barriers of 3.4 and 2.8 eV, respectively. Since the lateral hopping barrier on the H−Si(111) is 2.5 eV, surface hopping on dots larger than Si_{35} is expected to encounter barriers in the 2.5−3.4 eV range. This range would be larger for dots passivated with methyl and siloxane. Analysis also indicates that inward diffusion is more difficult on Si_{35} than for flat Si(111) with surface distortion on the dot adding an additional 0.9 eV to E_a^{inw}. In addition, while inward hopping could follow any adsorption event on Si(111), access to internal QD bonds must start from face bonds (Figure 2c,f). This requires that a specific chain of adsorption and diffusion steps be followed. Since E_a^{inw} = 2.8 eV for H−Si(111),[14] we expect that the inward barrier for any Si QDs with $d > 1.0$ nm is in the range of 2.8−3.7 eV.

This analysis of lateral and inward hopping indicates that O atoms will be frozen on the surface of otherwise defect-free passivated Si QDs, regardless of their size. Of course, surface dangling bonds could

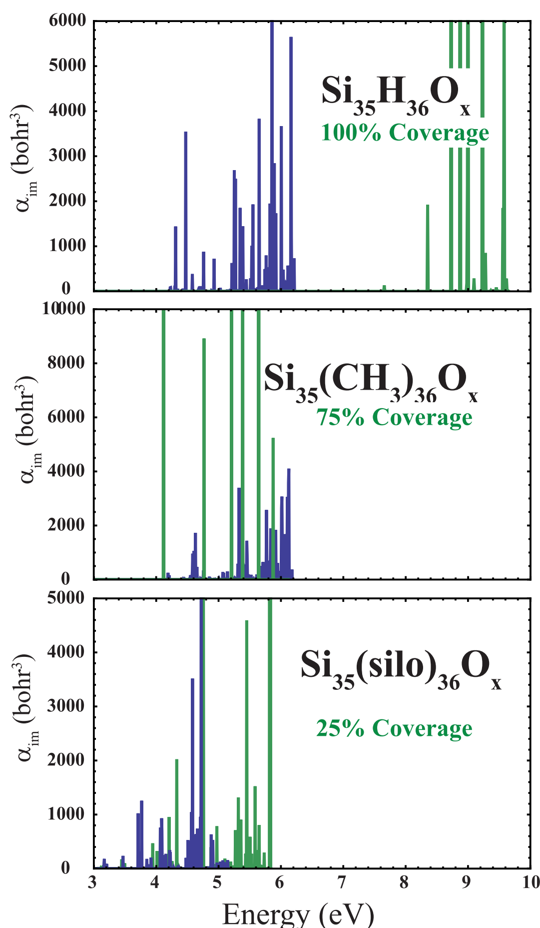

Figure 9. Optical absorption spectra of $Si_{35}H_{36}$, $Si_{35}(CH_3)_{36}$, and siloxane Si_{35} with no oxidation (blue) and predicted stable fraction of oxidation (green). Only 2 eV ranges at the absorption edges are shown.

TABLE 3. Quasiparticle HOMO/LUMO Levels of $Si_{35}H_{36}$, $Si_{35}(CH_3)_{36}$, and $Si_{35}(silo)_{36}$ with No Oxidation and Predicted Stable Fraction of Oxidation

Si QDs	HOMO (eV)	LUMO (eV)
$Si_{35}H_{36}$	−8.20	−1.46
$Si_{35}H_{36}O_{48}$	−9.81	1.58
$Si_{35}(CH_3)_{36}$	−7.03	−0.68
$Si_{35}(CH_3)_{36}O_{36}$	−8.54	−1.54
siloxane-Si_{35}	−7.90	−2.86
siloxane-$Si_{35}O_{12}$	−7.65	−2.76

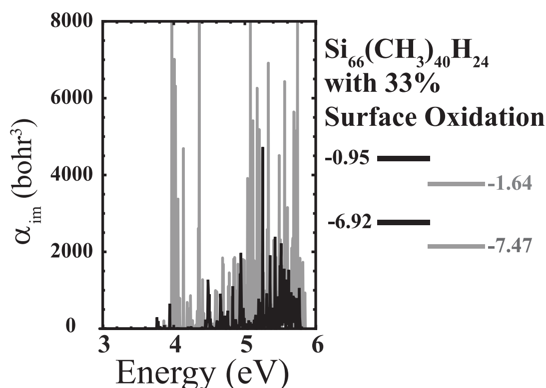

Figure 10. Optical absorption spectra of $Si_{66}(CH_3)_{40}H_{24}$ with no oxidation (black) and all apex bonds oxidized (gray). The inset shows the HOMO/LUMO levels of the corresponding systems.

change this dramatically, and previous theoretical analyses[31] have found much lower lateral and inward diffusion barriers within such settings.

Stability of the Optical and Electronic Properties of the Oxidized Si QDs. For small Si QDs, the effect of surface passivation on photoelectronic properties are crucial for their applications in photovoltaics, photoluminescences, *etc.* While the optical properties are mostly maintained regardless of these surface terminations, optical stability could be enhanced dramatically by silanization.[16,30]

According to our calculations, defect-free Si_{35} dots terminated with hydrogen, methyl, and siloxane will rapidly develop stable oxidized surface bonds with fractions of 100, 75, and 25%, respectively. It is therefore of interest to determine the effect of these oxygen atoms on the optical properties of such dots. Figure 9 summarizes the optical absorption spectra for all three terminations, and the corresponding quasiparticle (QP) energy levels of the highest occupied (HOMO) and the lowest unoccupied (LUMO) molecular orbitals are listed in Table 3. While the surface oxidation of $Si_{35}H_{36}$ blue shifts the optical gap by 3.2 eV, consistent with previous experiments,[6,32] the absorption edge is relatively stable in the partially oxidized dots (up to 75% coverage) with methyl termination. For the CH_3 passivation, interestingly, the oscillator strength near the absorption edge is strengthened significantly by oxidation; in addition, the HOMO and LUMO energies are lowered by 1.5 and 0.9 eV, respectively. In contrast, for the siloxane passivation, while the stability of the HOMO/LUMO level toward oxidation is greatly improved, as well, compared with H passivation, the change in absorption intensity near the optical gap is not as dramatic as that for methylated dots.

Although it is unlikely that the defect-free, methyl-passivated Si_{66} dots adsorb oxygen, we have investigated a representative structure with all apex bonds (33%) oxidized. Even at this very high level of oxidation, the change in optical gap is negligible, as shown in Figure 10. For this Si QD with a diameter of 1.2 nm, no significant absorption peaks are observed up to 4.5 eV, in reasonable agreement with experimental value of 4.3 eV for 1.8 nm Si QDs,[32] considering different dielectric environments. On the other hand, the strength of the optical absorption edge is enhanced considerably. Although the HOMO/LUMO levels decrease by 0.6/0.7 eV, a smaller shift is expected for lower O coverage. For dots bigger than Si_{66}, the optical and electronic properties were expected to change even less for the same fraction of O coverage.

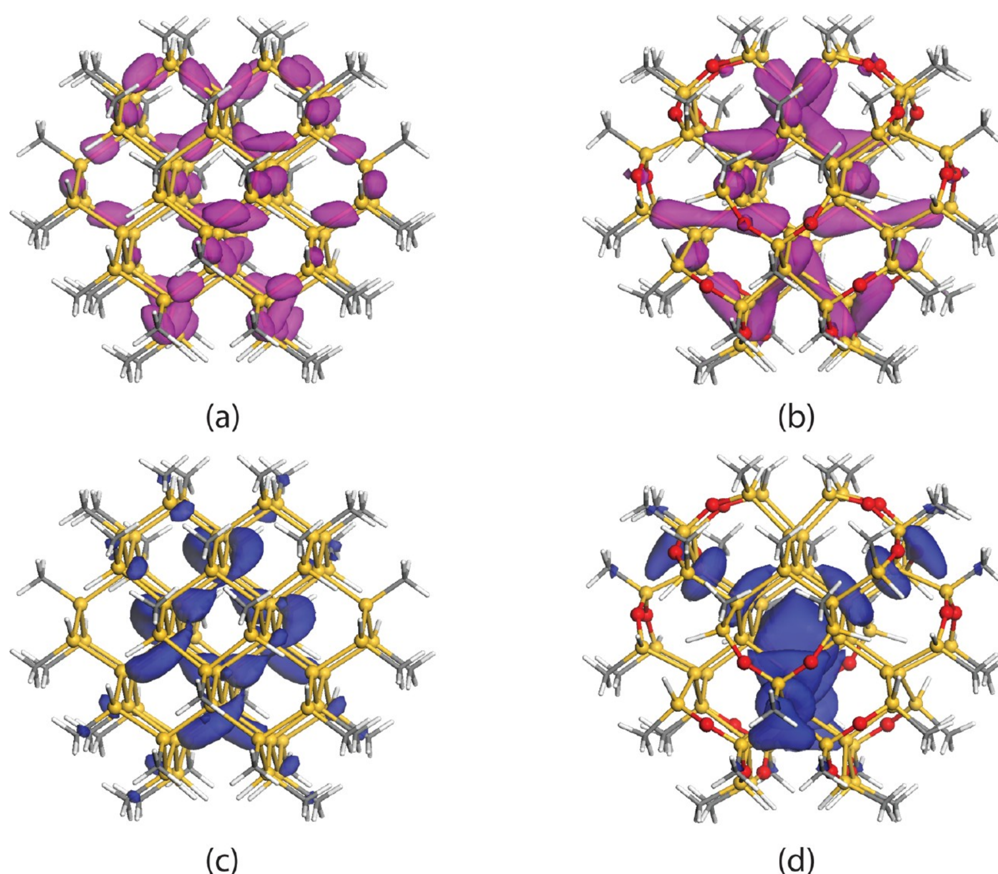

Figure 11. HOMO (Purple) and LUMO (blue) of $Si_{66}(CH_3)_{40}H_{24}$ without oxidation (a,c) and with (b,d) 33% oxygen coverage. The values of the isosurfaces are 0.01 $Å^{-3/2}$ for all cases.

The stability of optical and electronic properties against oxidation for methyl-terminated Si_{66} can be understood by the real space variation in excitonic wave functions due to the appearance of Si−O−Si bonds and the induced strain. The electron−hole interaction is known to be as large as ∼1 eV in these confined systems, thus the product of two associated QP wave functions can not well represent the excitonic wave function. Nevertheless, the distribution of the HOMO and LUMO orbitals, plotted in Figure 11, can still shed light on the modification in optical properties with respect to oxidation. When all of the corner bonds are oxidized, the HOMO of the dot shrinks to avoid the oxidized bonds, as shown in Figure 11b, while the LUMO becomes more delocalized, as shown in Figure 11d. The compensation of these two effects results in stable optical gap under oxidation, as well as high edge absorption intensity due to the larger overlap between the HOMO/LUMO wave functions. Besides, the more extended LUMO wave function might strengthen the electron coupling between neighboring dots, leading to higher electron mobility.

CONCLUSIONS

A first-principles analysis combined with previous experimental data suggests that methyl- and siloxane-coated Si QDs with diameters between 1.2 and 2.0 nm are of optimal size for resisting oxidation. The upper bound is determined by experiments which indicate that less than 0.1% of such dots will have defects,[27] and our computational study provides the lower bound below which the more open structures expose vulnerable Si bonds considerably. Surprisingly, methylated 1.2 nm dots have a minimum oxidation barrier of 2.4 eV, close to the 3.0 eV barrier offered by (defect-free) bulk CH_3−Si(111) surfaces.

Our computational investigation has also established that O atoms are essentially frozen in place for all of the Si QDs considered, with both lateral and inward diffusion barriers higher than 2 eV. This implies that unlikely oxidation events for dots within the optimum size range will be self-limited. Moreover, this small amount of inadvertent O adsorption has only a weak influence on optical gap while actually increasing the absorption intensity at the gap edge.

Current design paradigms seek to reduce oxidation rates by creating assemblies of relatively large Si QDs with long ligand terminations. While oxygen dissociation into the Si back bond sites is slowed within this paradigm, it comes at the price of hindering efficient charge transfer called for in both solar cells and LEDs. The results of the present study suggest an alternative

design paradigm in which the assemblies with small QDs and short ligands can be used to create robust QD assemblies with the prospect of excellent transport properties.[13]

METHODS

Our DFT calculations employed an all-electron approach with the exchange and correlation using the generalized gradient approximation (GGA) formulated by Perdew, Burke, and Ernzerhof (PBE[33]) and a real-space numerical atomic orbital basis implemented in Dmol package.[34] A double numeric plus d-orbital basis and an octupole expansion were used, which have been tested to be well converged. All ground state structures were relaxed until the maximum atomic force is less than 0.05 eV/Å.

To determine oxidation barriers, a synchronous transition (ST) state searching method[35] was used. In each ST circle, a series of single-point energy calculations were performed on a set of interpolated structures, and the configuration with maximum energy provides an estimate for the transition state geometry. A conjugate gradient (CG) minimization was followed by a quadratic synchronous transition (QST) analysis, and the process was repeated until the root-mean-square forces on all atoms are less than 0.27 eV/Å. To ensure that the SCF loops of interpolated structures converge, a tiny smearing of 0.027 eV was used. Then, a Hessian analysis was implemented on the estimated TS. Eventually, the final optimization of the TS and the associated energy barrier was carried out using the eigenvector following (EF) analysis[36] that applies a Newton-like algorithm to search for the energy maximum along a single (unstable) normal mode and the minimum along all others. The EF stops when at least two of the following criteria are satisfied: the maximum energy change is less than 2.7×10^{-5} eV, the maximum force is less than 0.05 eV/Å and the maximum displacement is less than 0.005 Å. The reliability of this suite of transition state methods for oxidation energy barriers on Si surfaces has been carefully examined in our previous publication.[14]

In order to obtain accurate optical properties, we applied the many-body perturbation theory within the *GW* approximation to obtain energy levels of QP states,[37,38] wherein the self-energy is estimated by the product of the single-particle Green function (*G*) and the screened Coulomb interaction (*W*). Excitonic effects and electron−hole interactions are then taken into account by constructing the two-particle Green functions using linear combinations of the calculated QP pairs. Then excitonic states and energies are computed *via* solving the Bethe−Salpeter equation (BSE),[38] and optical spectra are evaluated accordingly. Our *GW*-BSE calculations were carried out using the RGWBS package.[38] The grid spacing is 0.3 Å, while the boundary radius is 12 Å, ensuring that the surface-to-surface distances between mirror dots are larger than 8 Å, so that the unphysical dot-to-dot interaction is negligible. We performed non-self-consistent G_0W_F calculations, wherein the screened Coulomb interaction *W* is obtained within the time-dependent adiabatic local density approximation (TD-ALDA) along with the vertex correction. The quasiparticle states were obtained by direct diagonalization. The convergence with number of orbitals included in the basis for *GW*/BSE computations is carefully tested, and the results assert that 130 valence states and 130 conduction states are sufficient to obtain converged absorption spectra.

Conflict of Interest: The authors declare no competing financial interest.

Acknowledgment. This research is supported by the Renewable Energy Materials Research Science and Engineering Center (REMRSEC) and by startup funds from Colorado School of Mines (CSM) and the U.S. DOE early career research award (No. DE-SC-0006433). We also acknowledge the Golden Energy Computing Organization at the Colorado School of Mines for the use of resources acquired with financial assistance from the National Science Foundation and the National Renewable Energy Laboratories.

Supporting Information Available: Discussion of O_2 adsorption path on H-terminated Si QDs and uncertainties from geometric fluctuation. This material is available free of charge *via* the Internet at http://pubs.acs.org.

REFERENCES AND NOTES

1. Niesar, S.; Fabian, W.; Petermann, N.; Herrmann, D.; Riedle, E.; Wiggers, H.; Brandt, M. S.; Stutzmann, M. Efficiency Enhancement in Hybrid P3HT/Silicon Nanocrystal Solar Cells. *Green* **2011**, *1*, 339–350.
2. Beard, M. C.; Knutsen, K. P.; Yu, P.; Luther, J. M.; Song, Q.; Metzger, W. K.; Ellingson, R. J.; Nozik, A. J. Multiple Exciton Generation in Colloidal Silicon Nanocrystals. *Nano Lett.* **2007**, *7*, 2506–2512.
3. Hofmeister, H.; Huisken, F.; Kohn, B. Lattice Contraction in Nanosized Silicon Particles Produced by Laser Pyrolysis of Silane. *Eur. Phys. J. D* **1999**, *9*, 137–140.
4. Yang, D.; Gillet, J.; Meunier, M.; Sacher, E. Room Temperature Oxidation Kinetics of Si Nanoparticles in Air, Determined by X-ray Photoelectron Spectroscopy. *J. Appl. Phys.* **2005**, *97*, 024303.
5. Higashi, G.; Becker, R.; Chabal, Y.; Becker, A. Comparison of Si(111) Surfaces Prepared Using Aqueous-Solutions of NH4F *versus* HF. *Appl. Phys. Lett.* **1991**, *58*, 1656–1658.
6. Ledoux, G.; Gong, J.; Huisken, F. Effect of Passivation and Aging on the Photoluminescence of Silicon Nanocrystals. *Appl. Phys. Lett.* **2001**, *79*, 4028–4030.
7. Umezu, I.; Sugimura, A.; Makino, T.; Inada, M.; Matsumoto, K. Oxidation Processes of Surface Hydrogenated Silicon Nanocrystallites Prepared by Pulsed Laser Ablation and Their Effects on the Photoluminescence Wavelength. *J. Appl. Phys.* **2008**, *103*, 024305.
8. Shinoda, K.; Yanagisawa, S.; Sato, K.; Hirakuri, K. *J. Cryst. Growth* **2006**, *288*, 84–86.
9. Ledoux, G.; Guillois, O.; Porterat, D.; Reynaud, C.; Huisken, F.; Kohn, B.; Paillard, V. Photoluminescence Properties of Silicon Nanocrystals as a Function of Their Size. *Phys. Rev. B* **2000**, *62*, 15942–15951.
10. Wolkin, M. V.; Jorne, J.; Fauchet, P. M.; Allan, G.; Delerue, C. Electronic States and Luminescence in Porous Silicon Quantum Dots: The Role of Oxygen. *Phys. Rev. Lett.* **1999**, *82*, 197–200.
11. Kabashin, A.; Sylvestre, J.; Patskovsky, S.; Meunier, M. Correlation between Photoluminescence Properties and Morphology of Laser-Ablated Si/SiOx Nanostructured Films. *J. Appl. Phys.* **2002**, *91*, 3248–3254.
12. Lin, Z.; Franceschetti, A.; Lusk, M. T. Size Dependence of the Multiple Exciton Generation Rate in CdSe Quantum Dots. *ACS Nano* **2011**, *5*, 2503–2511.
13. Lin, Z.; Li, H.; Franceschetti, A.; Lusk, M. T. Efficient Exciton Transport between Strongly Quantum-Confined Silicon Quantum Dots. *ACS Nano* **2012**, *6*, 4029–4038.
14. Li, H.; Wu, Z.; Lusk, M. First Principles Analysis of the Initial Oxidation of Si(001) and Si(111) Surfaces Terminated with H and CH_3. *J. Chem. Phys.* **2012**, *136*, 064507.
15. Zhang, X.; Garfunkel, E.; Chabal, Y. J.; Christman, S. B.; Chaban, E. E. Stability of HF-Etched Si(100) Surfaces in Oxygen Ambient. *Appl. Phys. Lett.* **2001**, *79*, 4051–4053.
16. Zou, J.; Baldwin, R.; Pettigrew, K.; Kauzlarich, S. Solution Synthesis of Ultrastable Luminescent Siloxane-coated Silicon Nanoparticles. *Nano Lett.* **2004**, *4*, 1181–1186.
17. Li, Z. F.; Swihart, M. T.; Ruckenstein, E. Luminescent Silicon Nanoparticles Capped by Conductive Polyaniline through the Self-Assembly Method. *Langmuir* **2004**, *20*, 1963–1971.
18. Zou, J.; Kauzlarich, S. M. Functionalization of Silicon Nanoparticles *via* Silanization: Alkyl, Halide and Ester. *J. Cluster Sci.* **2008**, *19*, 341–355.
19. Anderson, I. E.; Shircliff, R. A.; Macauley, C.; Smith, D. K.; Lee, B. G.; Agarwal, S.; Stradins, P.; Collins, R. T. Silanization of

Low-Temperature-Plasma Synthesized Silicon Quantum Dots for Production of a Tunable, Stable, Colloidal Solution. *J. Phys. Chem. C* **2012**, *116*, 3979–3987.
20. Yang, Y.; Rodriguez-Cordoba, W.; Xiang, X.; Lian, T. Strong Electronic Coupling and Ultrafast Electron Transfer between PbS Quantum Dots and TiO_2 Nanocrystalline Films. *Nano Lett.* **2012**, *12*, 303–309.
21. Williams, K. J.; Tisdale, W. A.; Leschkies, K. S.; Haugstad, G.; Norris, D. J.; Aydil, E. S.; Zhu, X.-Y. Strong Electronic Coupling in Two-Dimensional Assemblies of Colloidal PbSe Quantum Dots. *ACS Nano* **2009**, *3*, 1532–1538.
22. Pereira, R. N.; Rowe, D. J.; Anthony, R. J.; Kortshagen, U. Oxidation of Freestanding Silicon Nanocrystals Probed with Electron Spin Resonance of Interfacial Dangling Bonds. *Phys. Rev. B* **2011**, *83*, 155327.
23. Niesar, S.; Stegner, A. R.; Pereira, R. N.; Hoeb, M.; Wiggers, H.; Brandt, M. S.; Stutzmann, M. Defect Reduction in Silicon Nanoparticles by Low-Temperature Vacuum Annealing. *Appl. Phys. Lett.* **2010**, *96*, 193112.
24. Dohnalova, K.; Kusova, K.; Pelant, I. Time-Resolved Photoluminescence Spectroscopy of the Initial Oxidation Stage of Small Silicon Nanocrystals. *Appl. Phys. Lett.* **2009**, *94*, 211903.
25. Pi, X. D.; Mangolini, L.; Campbell, S. A.; Kortshagen, U. Room-Temperature Atmospheric Oxidation of Si Nanocrystals after HF Etching. *Phys. Rev. B* **2007**, *75*, 085423.
26. Mangolini, L.; Thimsen, E.; Kortshagen, U. High-Yield Plasma Synthesis of Luminescent Silicon Nanocrystals. *Nano Lett.* **2005**, *5*, 655–659.
27. Niesar, S.; Pereira, R. N.; Stegner, A. R.; Erhard, N.; Hoeb, M.; Baumer, A.; Wiggers, H.; Brandt, M. S.; Stutzmann, M. Low-Cost Post-Growth Treatments of Crystalline Silicon Nanoparticles Improving Surface and Electronic Properties. *Adv. Funct. Mater.* **2012**, *22*, 1190–1198.
28. Lu, Z.; Sacher, E.; Yelon, A. Kinetics of the Room-Temperature Air Oxidation of Hydrogenated Amorphous-Silicon and Crystalline Silicon. *Philos. Mag. B* **1988**, *58*, 385–388.
29. Mastronardi, M. L.; Maier-Flaig, F.; Faulkner, D.; Henderson, E. J.; KÃijbel, C.; Lemmer, U.; Ozin, G. A. Size-Dependent Absolute Quantum Yields for Size-Separated Colloidally-Stable Silicon Nanocrystals. *Nano Lett.* **2012**, *12*, 337–342.
30. Yang, C.; Bley, R.; Kauzlarich, S.; Lee, H.; Delgado, G. Synthesis of Alkyl-Terminated Silicon Nanoclusters by a Solution Route. *J. Am. Chem. Soc.* **1999**, *121*, 5191–5195.
31. Eyre, R. J.; Goss, J. P.; Briddon, P. R. Effect of Progressive Oxidation on the Optical Properties of Small Silicon Quantum Dots: A Computational Study. *Phys. Rev. B* **2008**, *77*, 245407.
32. Shirahata, N. Colloidal Si Nanocrystals: A Controlled Organic−Inorganic Interface and Its Implications of Color-Tuning and Chemical Design toward Sophisticated Architectures. *Phys. Chem. Chem. Phys.* **2011**, *13*, 7284–7294.
33. Perdew, J. P.; Wang, Y. Accurate and Simple Analytic Representation of the Electron-Gas Correlation Energy. *Phys. Rev. B* **1992**, *45*, 13244–13249.
34. Delley, B. An All-Electron Numerical-Method For Solving the Local Density Functional for Polyatomic-Molecules. *J. Chem. Phys.* **1990**, *92*, 508–517.
35. Halgren, T. A.; Lipscomb, W. N. The Synchronous-Transit Method for Determining Reaction Pathways and Locating Molecular Transition States. *Chem. Phys. Lett.* **1977**, *49*, 225–232.
36. Mauro, J.; Loucks, R.; Balakrishnan, J. A Simplified Eigenvector-Following Technique for Locating Transition Points in an Energy Landscape. *J. Phys. Chem. A* **2005**, *109*, 9578–9583.
37. Aulbur, W. G.; Jonsson, L.; Wilkins, J. W. In Quasiparticle Calculations in Solids. *Solid State Physics-Advances in Research and Applications*; Ehrenreich, H., Spaepen, F., Eds.; Academic Press: New York, 1999; Vol. 54; pp 1−218.
38. Tiago, M. L.; Chelikowsky, J. R. Optical Excitations in Organic Molecules, Clusters, and Defects Studied by First-Principles Green's Function Methods. *Phys. Rev. B* **2006**, *73*, 205334.